

^{1,2}Hyung-Gyu Lim, ³John P. Dunne, ³Charles A. Stock, ^{3,4}Paul Ginoux, ^{3,4}Jasmin G. John, and ³John Krasting

¹AOS program, Princeton University, NJ, USA ²Scripps Institution of Oceanography, UC San Diego, CA, USA ³NOAA/OAR/Geophysical Fluid Dynamics Laboratory, Princeton, NJ, USA, ⁴NOAA/OAR/Atlantic Oceanographic and Meteorological Laboratory, Miami, FL, USA

Motivation

- ✓ New generation GFDL-ESM4.1 (*Dunne et al 2020; Stock et al 2020*)
 - Better fidelity of ENSO simulation (*Planton et al 2021*)
 - Dynamic dust-iron deposition in land to ocean delivery (*Evans et al 2016*)

a) Performance b) Telecon. c) Processes

* = CMIP6 model

(*Planton et al 2021*)

Q) GFDL-ESM4.1 do better ENSO-CHL coupling?
Evaluating dominant factor whether **physical driven** or iron cycling driven?

Datasets

- *piControl simulations from two generations of GFDL earth system models: years 1001–1100 of ESM2M; years 501–645 of ESM4.1*
 - *Satellite-derived ocean color for chlorophyll estimation: the European Space Agency Ocean Colour Climate Change Initiative project (ESA-CCI) version 4.2*
 - *NOAA Extended Reconstructed SST version 5 (ERSST v5).*
 - *Vertical temperature profiles: version 3.4.2 of the Simple Ocean Data Assimilation (SODA)*
 - *Two satellite-derived aerosol optical thicknesses: NOAA Climate Data Record (CDR) of AVHRR Daily and Monthly Aerosol Optical Thickness (AOT) over Global Oceans, Version 3.0; SeaWiFS Deep Blue Level 3 monthly product which contains monthly global gridded ($1^{\circ} \times 1^{\circ}$) data derived from SeaWiFS Deep Blue Level 3 daily gridded data (Hsu et al., 2013).*

Methods

ESM4.1-static run

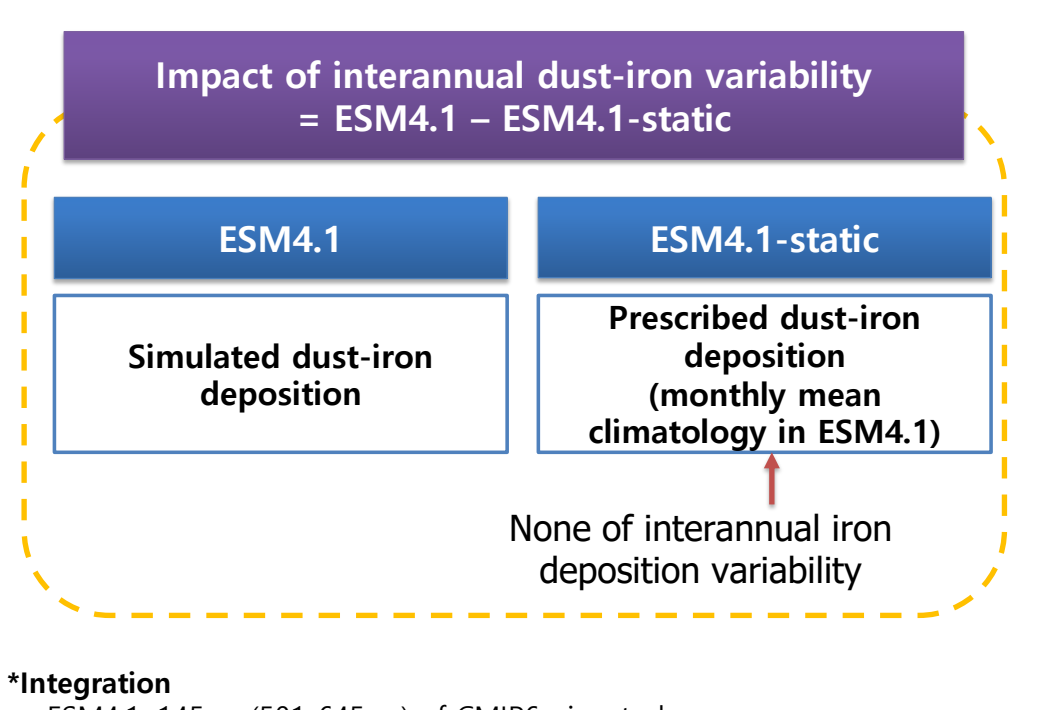
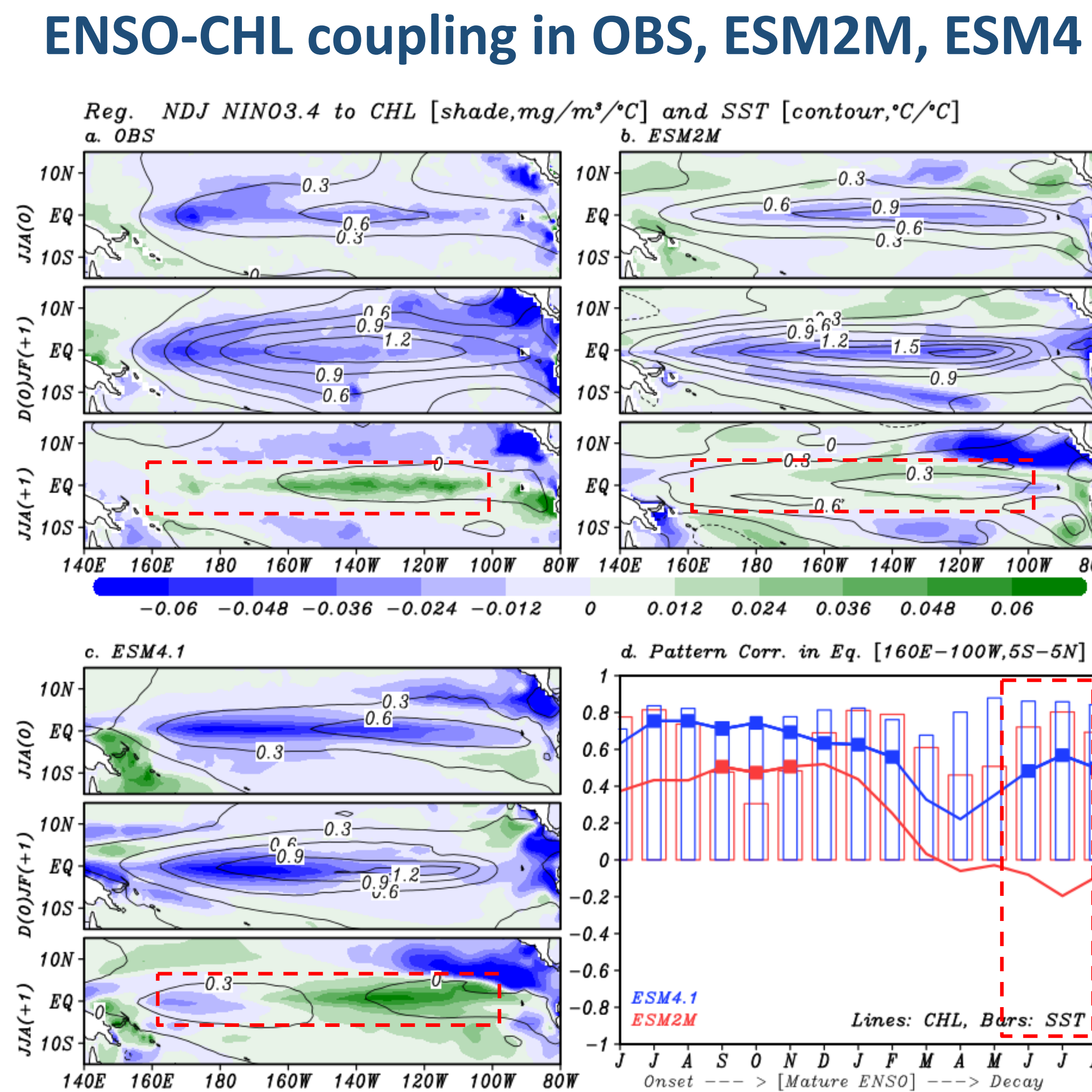


Figure 1. Spatially resolved ENSO-regression of temperature (contours, $^{\circ}$ C/ $^{\circ}$ C) and chlorophyll concentration (shading, mg/m³/ $^{\circ}$ C) anomalies against ENSO in (a) satellite, SODA, (b) ESM2M, and (c) ESM4.1. Values are shown for ENSO onset (JJA[0]), mature state (D[0]JF[+1]), and decay (JJA+1) ENSO states; (d) pattern correlations of ESM2M (red) and ESM4.1 (blue) regression coefficients (i.e., panels b and c) with SODA (bars) and satellite chlorophyll (lines; square symbols denote the Student's t-test statistical significance at 95% confidence level) regression coefficients (i.e., panel a) in the EP (160° E– 100° W, 5° N– 5° S).



Post El Niño Iron rebound

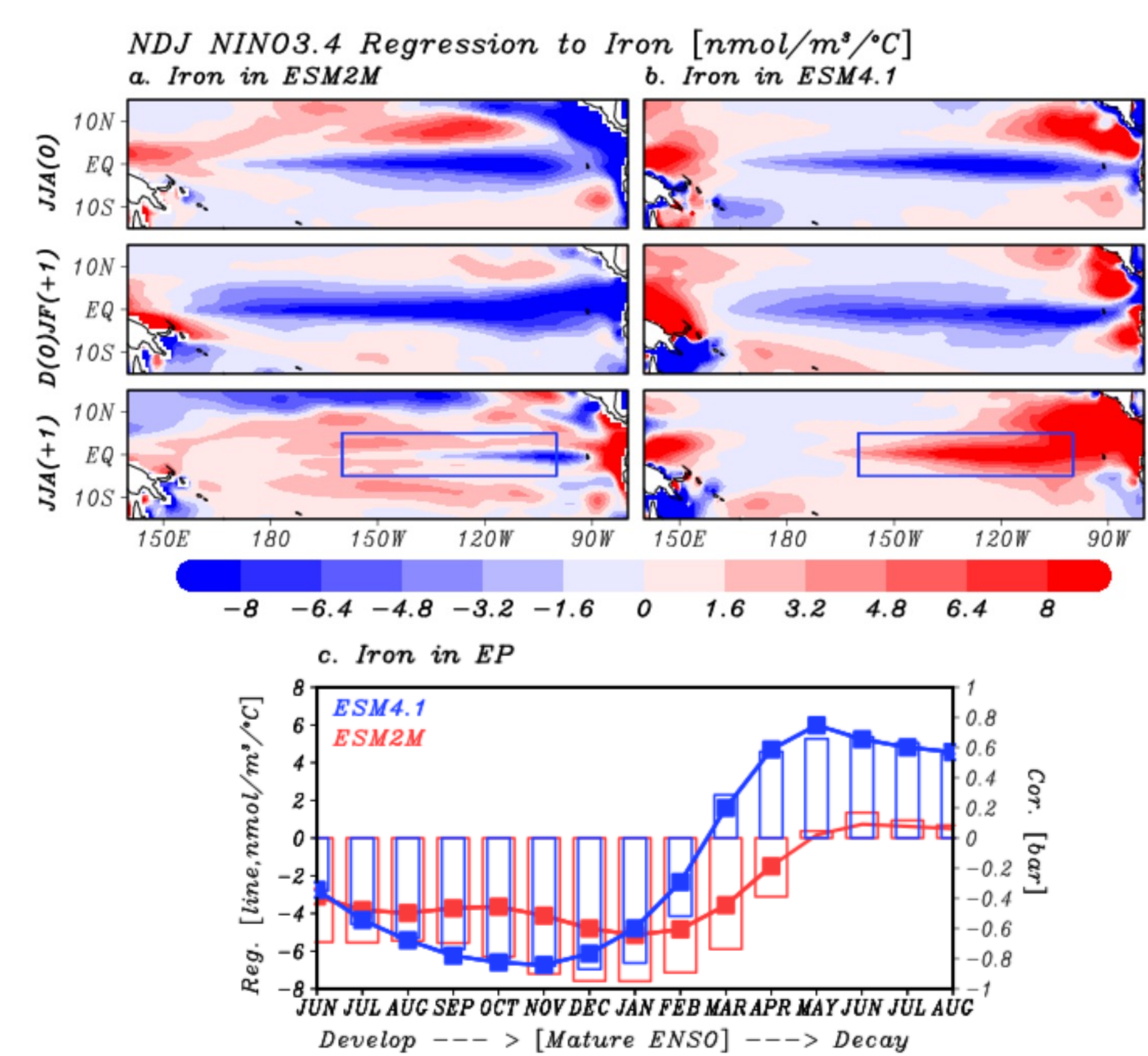


Figure 2. ENSO-regressed patterns in spatially resolved surface iron concentration anomalies ($\text{nmol/m}^3/\text{ }^\circ\text{C}$) in (a) ESM2M and (b) ESM4.1. (c) lead-lag ENSO regression (lines; square symbols denote the Student's *t*-test statistical significance at 95% confidence level) and correlation (bar) coefficients in regional monthly iron concentration anomalies in the eastern FP ($160\text{ }^\circ\text{--}100\text{ }^\circ\text{W}, 5\text{ }^\circ\text{S}\text{--}5\text{ }^\circ\text{N}$).

Atmospheric Driver

- NDJ NINO3.4 Reg. Dynamic dust effect (ESM4.1 – ESM4.1 – static)*

a. Iron Dep. at EP [umol/m³/yr/°C]

b. Cor. Iron Dep. & Obs. AOT at EP

Mechanism: El Niño to dust-iron

Westerly wind burst and El Niño onset

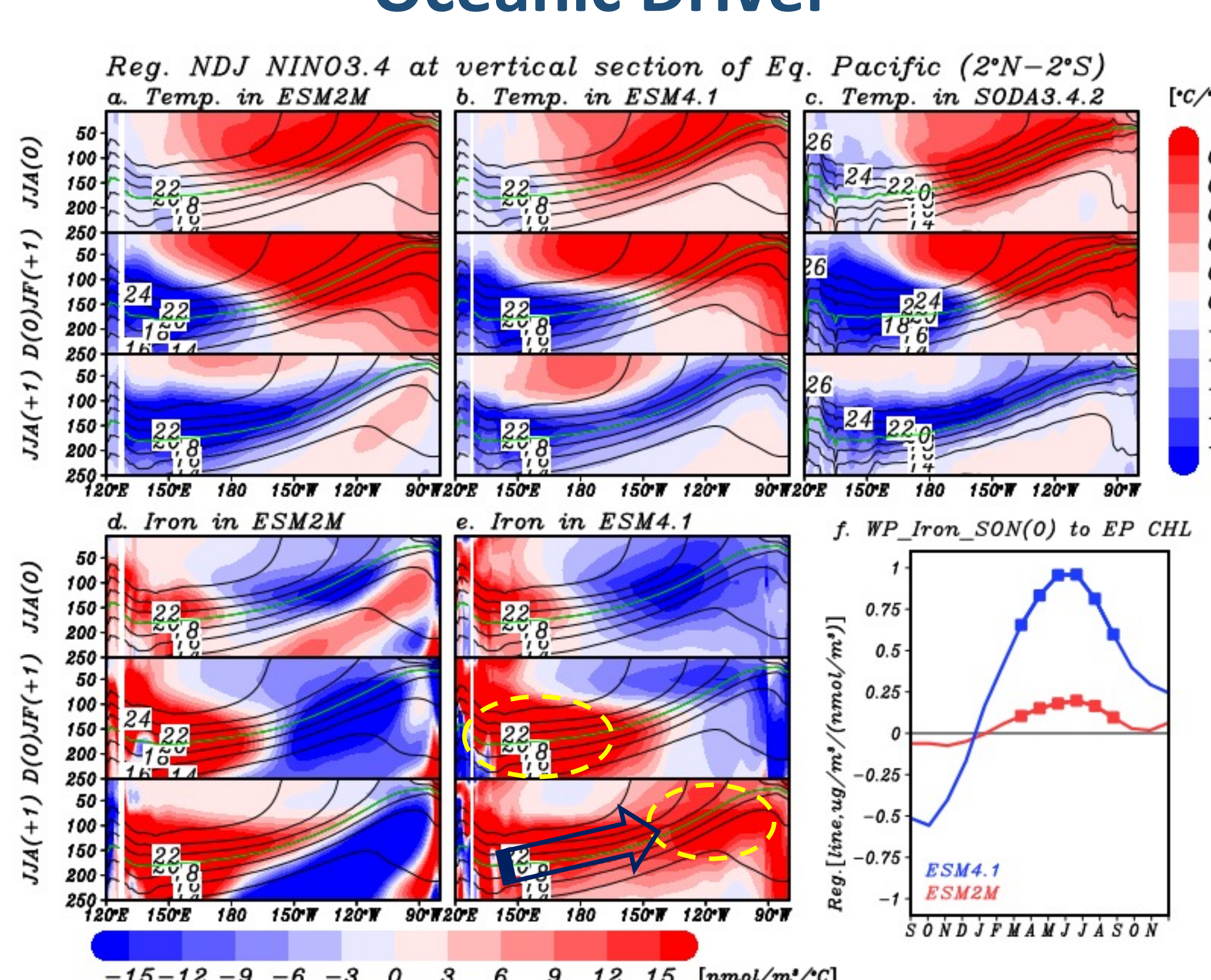
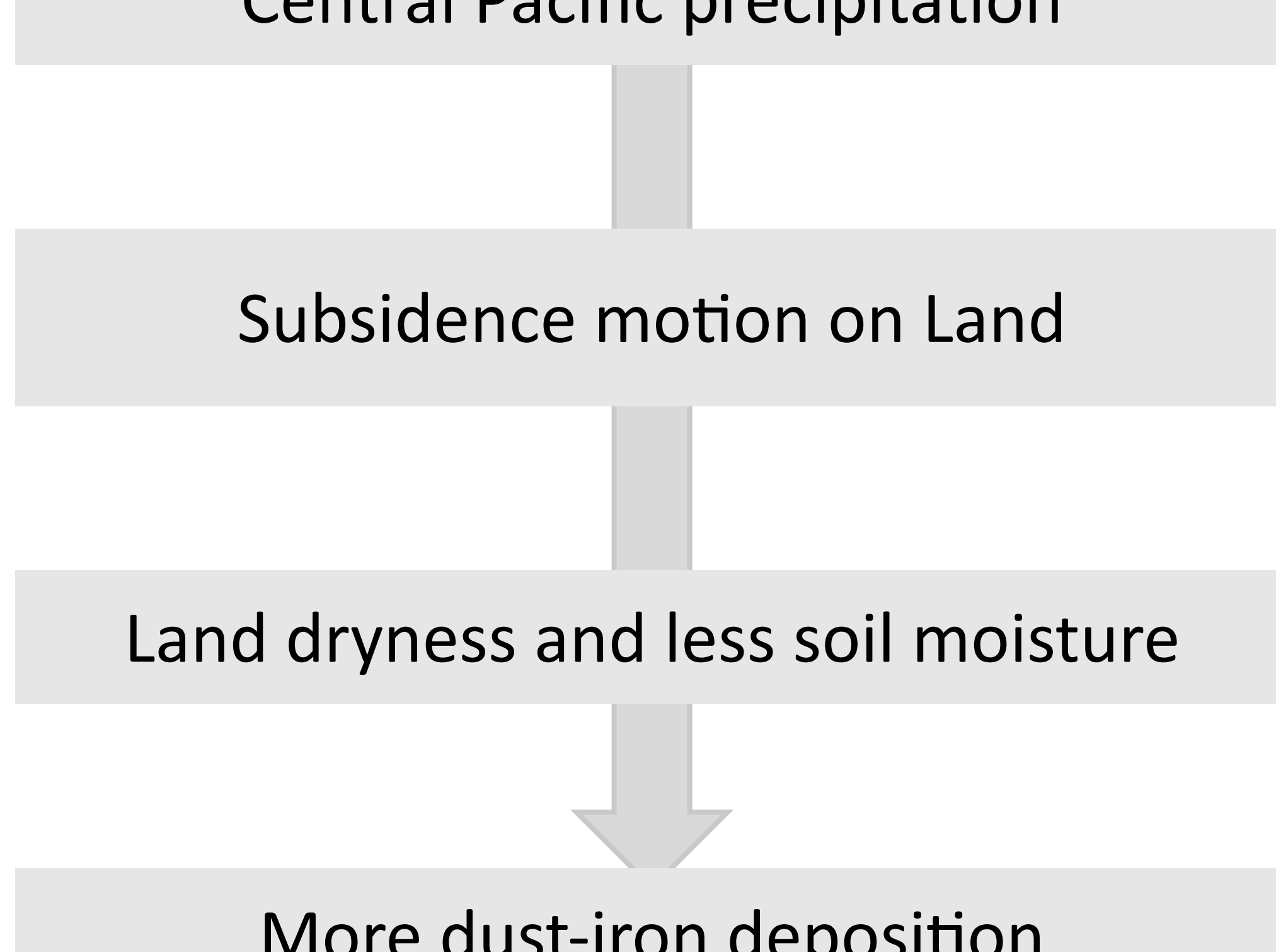


Figure 3. ENSO-regressed coefficients of vertical sections of equatorial temperature anomalies in (a) ESM2M, (b) ESM4.1, (c) SODA and dissolved iron concentration anomalies (shading) in (d) ESM2M, (e) ESM4.1. The temperature climatology from each model and SODA has been overlaid (contours) to aid interpretation and 20 °C isotherm (green line) at equator (2 °N–2 °S). (f) Regressed coefficients (square symbols denote the statistical significance at 95% confidence level) of iron concentration anomalies in the WP subsurface region averaged in (130 °–160 °E, 2 °N–2 °S, 100–200 m depth) at SON(0) against the eastern EP surface (160 °–100 °W, 5 °S–5 °N) monthly chlorophyll concentration anomalies simulated in ESM2M (red) and ESM4.1 (blue).



Conclusion

Better capturing post-El Niño CHL rebound pattern in GFDL-ESM4.1 (*Fig. 1*)

- Much more iron supply (*Fig. 2*) in post-El Niño event into the eastern equatorial Pacific in ESM4.1 than ESM2M
 - **Oceanic driver (*Fig. 3*): Iron trapping and its propagation via equatorial undercurrent (Dominant factor to ENSO-CHL rebound)
 - Atmospheric driver (*Fig. 4*): Less precipitation on land increases dust-iron deposition (Argument factor to ENSO-CHL sensitivity)
 - The chlorophyll rebound in GFDL-ESM4.1 may provide a key source of resilience to marine ecosystem simulation in the equatorial Pacific for management of living marine resources.

Further descriptions and references at:

Lim, H.-G., Dunne, J. P., Stock, C. A., Ginoux, P., John, J. G., & Krasting, J. (2022). *Oceanic and atmospheric drivers of post-El-Niño chlorophyll rebound in the equatorial Pacific*. Geophysical Research Letters, 49, e2021GL096113. <https://doi.org/10.1029/2021GL096113>